MID-INFRARED SPECTROSCOPY OF HIGH-REDSHIFT OBSCURED QUASARS

ALEJO MARTÍNEZ-SANSIGRE,[1] MARK LACY,[2] ANNA SAJINA,[2] AND STEVE RAWLINGS[3]

ABSTRACT

We present mid-infrared observations of 18 sources from a sample of 21 $z \sim 2$ radio-intermediate obscured (type 2) quasars. The mid-infrared spectra of the sources are continuum dominated, and 12 sources show deep silicate absorption with $\tau_{9.7} \sim 1$–2. Combining mid-infrared and optical spectra, we achieve 86% spectroscopic completeness which allows us to confirm that most (63^{+14}_{-22}%) $z \sim 2$ radio-intermediate quasars are obscured. The new spectra also prove that many high-redshift type 2 quasars do not show any rest-frame ultraviolet emission lines. From the 18 individual mid-infrared spectra, we classify most of the sources into three subsamples: those with hints of the 7.7 and 6.2 μm polyaromatic hydrocarbons (3/18 sources show PAHs; subsample A), those with an excess of emission around 8 μm but no hint of the 6.2 μm PAH (7/18 cases; subsample B), and pure-continuum sources with no visible excess (4/18 sources; subsample C). The remaining 4/18 sources have spectra that are featureless or too noisy for any features to be visible. In subsample A, averaging the spectra leads to a statistical detection of both 6.2 and 7.7 μm PAHs over the continuum, with the strength of the 7.7 μm PAH comparable to that of submillimeter-selected galaxies (SMGs) at similar redshifts. These sources are in a phase of coeval growth of a supermassive black hole and a host galaxy.

Subject headings: galaxies: active — galaxies: high-redshift — galaxies: nuclei — galaxies: starburst — infrared: galaxies — quasars: general

1. INTRODUCTION

The correlations between galaxy and central supermassive black hole properties found in the local universe (Magorrian et al. 1998; Ferrarese & Merritt 2000) have led to notions that the growth of both must be intimately related. A fraction of the gas fueling star formation is believed to reach the black hole, which will grow by accretion during an obscured quasar phase (Fabian 1999), and is expected to develop winds or jets that eventually become powerful enough to expel the gas, preventing any further star formation (Silk & Rees 1998). This feedback process is needed to avoid forming more stars than are seen around local dormant black holes (Benson et al. 2003), but few compelling examples of this phase have been reported to date.

Quasars are believed to be viewed as obscured or unobscured depending on the orientation of the line of sight with respect to the axis of symmetry and the dusty "torus" surrounding the accretion disk (Antonucci 1993), yet the population of powerful obscured quasars have remained elusive. Since most of the growth of supermassive black holes is obscured by dust, optical surveys miss this phase completely, and X-ray surveys miss a significant fraction due to associated gas column. Recently, mid-infrared surveys have been able to find obscured active galactic nuclei (AGNs) in large numbers, but care must be taken to separate AGNs from star-forming galaxies. This can be achieved by making use of the particular mid-infrared colors of AGNs (e.g., Lacy et al. 2004; Alonso-Herrero et al. 2006) or using a combination of mid-infrared and radio data (e.g., Martínez-Sansigre et al. 2005; Donley et al. 2005). Indeed, from these surveys it seems that a large fraction of obscured AGNs are undetected in X-rays (e.g., Donley et al. 2005; Alonso-Herrero et al. 2006; Lacy et al.

2007; Martínez-Sansigre et al. 2007), and that mid-infrared-selected samples give a more complete picture than X-ray-selected samples. Some obscured quasars, however, do not show even the narrow emission lines expected if the central regions are obscured at certain angles by a torus (see Martínez-Sansigre et al. 2005, 2006b), some have evidence for dust in front of the narrow-line region (Brand et al. 2007), and radio observations suggest that in some cases the radio jet is closely aligned with the observer's line of sight (Martínez-Sansigre et al. 2006a; Sajina et al. 2007; H.-R. Klöckner et al. 2008, in preparation), observations which are incompatible with the scenario of all obscuration being caused by the torus around the accretion disk.

The existence of objects which are not easily explained in the torus model has led to the suggestion that, in many cases, dust on scales of kiloparsecs is responsible for the obscuration. Since young stars are born in dusty regions, it is possible that in these sources the host galaxy is undergoing an episode of star formation. Mid-infrared spectroscopy gives a clean method of looking for star formation in the form of emission from complex molecules such as polycyclic aromatic hydrocarbons (PAHs; e.g., Aitken & Roche 1985; Roche et al. 1991). These molecules are excited by ultraviolet photons from young stars, but destroyed by the hard radiation of an AGN out to ~ 100 pc–1 kpc scales (e.g., Voit 1991; Siebenmorgen et al. 2004). Thus, detection of the PAH emission bands can only be attributed to star formation and not to excitation by an AGN.

If obscured and unobscured quasars are identical types of objects viewed at a different orientation, then the properties of their host galaxies, such as the PAH luminosity, should be identical on average. In a detailed study of local AGNs, Clavel et al. (2000) found that indeed the PAH luminosities of Seyfert 1 and Seyfert 2 AGNs are statistically indistinguishable, and that the observed differences between the Seyfert 1 and 2 spectra are due to the different contrast between the PAHs and the continuum, the latter being weaker for Seyfert 2s.

In this paper we present the results of mid-infrared spectroscopy of a sample of radio-intermediate obscured (type 2) quasars, which show either narrow lines or no emission lines in their optical

[1] Max-Planck-Insitut für Astronomie, Königstuhl 17, D-69117 Heidelberg, Germany; ams@mpia.de.
[2] *Spitzer* Science Center, California Institute of Technology, MS 220-6, 1200 East California Boulevard, Pasadena, CA 91125; mlacy@ipac.caltech.edu, sajina@ipac.caltech.edu.
[3] Astrophysics, Department of Physics, University of Oxford, Keble Road, Oxford OX1 3RH, UK; sr@astro.ox.ac.uk.

TABLE 1
MEASURED AND DERIVED PROPERTIES OF OUR SAMPLE OF OBSCURED QUASARS

Name	R.A. (J2000.0)	Decl. (J2000.0)	z[a]	Optical Spectrum[b]	Radio Spectrum[c]	N_{LL1}[d]	N_{LL2}[d]	Subsample[e]
AMS 01........................	17 13 11.17	+59 55 51.5	...	B	SS	10	10	N.F.
AMS 02........................	17 13 15.88	+60 02 34.2	1.8	B	SS	10	10	B
AMS 03........................	17 13 40.19	+59 27 45.8	2.698	NL	SS	0	0	N.O.
AMS 04........................	17 13 40.62	+59 49 17.1	1.782	NL	SS	10	10	B
AMS 05........................	17 13 42.77	+59 39 20.2	2.850[f]	NL	GP	3	3	C
AMS 06........................	17 13 43.91	+59 57 14.6	1.8	B	SS	6	6	B
AMS 07........................	17 14 02.25	+59 48 28.8	...	B	FS	10	10	N.F.
AMS 08........................	17 14 29.67	+59 32 33.5	1.979	NL	...	9	9	B
AMS 09........................	17 14 34.87	+58 56 46.4	2.1	B	SS	8	6	B
AMS 10........................	17 16 20.08	+59 40 26.5	...	B	SS	10	10	N.F.
AMS 11........................	17 18 21.33	+59 40 27.1	1.6	B	SS	10	10	A
AMS 12........................	17 18 22.65	+59 01 54.3	2.767	NL	SS	0	0	N.O.
AMS 13........................	17 18 44.40	+59 20 00.8	1.974	NL	SS	3	2	C
AMS 14........................	17 18 45.47	+58 51 22.5	1.794	NL	SS	3	2	C
AMS 15........................	17 18 56.93	+59 03 25.0	2.1	B	FS	10	10	B
AMS 16........................	17 19 42.07	+58 47 08.9	4.169	NL	GP	0	0	N.O.
AMS 17........................	17 20 45.17	+58 52 21.3	3.137	NL	SS	8	6	A
AMS 18........................	17 20 46.32	+60 02 29.6	1.6[f]	B	FS	10	10	B
AMS 19........................	17 20 48.00	+59 43 20.7	2.3	B	FS	5	5	C
AMS 20........................	17 20 59.10	+59 17 50.5	...	B	GP	10	10	N.F.
AMS 21........................	17 21 20.09	+59 03 48.6	1.8	B	SS	10	10	A

NOTE.—Units of right ascension are hours, minutes, and seconds, and units of declination are degrees, arcminutes, and arcseconds.

[a] The redshifts are all spectroscopic. Redshifts with three decimal places are from optical spectroscopy, from Martínez-Sansigre et al. (2006b), except AMS 05 and AMS 18, as discussed in the Appendix, while those with only one decimal place are from mid-infrared spectroscopy.

[b] Summary of optical spectroscopy properties. B = blank spectrum. NL = narrow lines.

[c] Summary of radio spectral properties from Martínez-Sansigre et al. (2006a). SS = steep spectrum. FS = flat spectrum. GP = gigahertz-peaked source.

[d] The expressions N_{LL1} and N_{LL2} are the number of cycles used in each of the LL1 and LL2 orders, respectively. All cycles have a duration of 120 s. AMS 03, AMS 12, and AMS 16 were not observed with IRS due to their high redshift.

[e] For AMS 01, AMS 07, AMS 10, and AMS 20, it was not possible to identify securely any features and a redshift, so they are labeled as having no features (N.F.). Obviously, AMS 03, AMS 12, and AMS 16 cannot be classified into any subsample, since they were not observed (N.O.). For the rest of the sources, the letter of which subsample each source belongs is quoted.

[f] As discussed in the Appendix, these two redshifts have been revised. The new redshift for AMS 05 is from optical spectroscopy (D. Smith 2007, private communication), while for AMS 18 it is from mid-infrared spectroscopy.

(rest-frame ultraviolet) spectra. Throughout this paper we assume a ΛCDM cosmology with $h = H_0/(100 \text{ km s}^{-1} \text{ Mpc}^{-1}) = 0.7$, $\Omega_m = 0.3$, $\Omega_\Lambda = 0.7$.

2. OBSERVATIONS AND DATA REDUCTION

Our sample of radio-intermediate obscured quasars, first presented in Martínez-Sansigre et al. (2005), was observed using the Infrared Spectrograph (IRS) instrument (Houck et al. 2004) on board the *Spitzer Space Telescope* (Werner et al. 2004; GO-30634 and archival data). At $z \gtrsim 1$, the brightest PAH lines, as well as the silicate features, are all redshifted out of the range covered by the Short-Low module (5.2–14.5 μm). Therefore, only the low-resolution, long-wavelength detector was used (Long-Low), with both orders, giving coverage in the spectral range 14–38 μm. However, due to the high noise above 35 μm, we only make use of the range 14–35 μm. The number of cycles each source was observed for is shown in Table 1. Each cycle involves two nodded positions, with an individual cycle duration of 120 s at each position. Note that three sources were not observed due to their high redshifts (AMS 03, AMS 12, and AMS 16).

The basic calibration data (BCD) from the *Spitzer* Science Center IRS pipeline were then combined by subtracting nodded pairs, and median combining the pairs. The number of nodded pairs combined in this way varies between 2 and 10, depending on the source (see Table 1). Both mean and median combining were tried, and for most sources the resulting spectra were almost indistinguishable. Mean combining led to slightly better signal-to-noise ratio (S/N) spectra in the smooth regions, but median combining generally proved better at removing spikes of noise. Given the low S/N for most of our spectra, median combining was chosen.

The two-dimensional spectra were cleaned of rogue pixels using IRSCLEAN,[4] and one-dimensional spectra were extracted using the optimal extraction in SPICE.[5] For the optimal extraction, an uncertainty file was first created from the frame-to-frame variance of each pixel, using the 440 BCD files of our own GO program. This uncertainty file was scaled to the correct exposure time for each source, and is overlaid in Figure 1. All 18 sources are detected in the reduced data.

3. MID-INFRARED SPECTRA

3.1. *Spectral Characteristics*

The mid-infrared spectra allow us to obtain spectroscopic redshifts for a further eight sources, confirming that 17 out of 21 sources in our sample lie at $z \geq 1.6$. Contamination by pure starbursts is unlikely, since the mid-infrared spectra are characteristic of AGN-dominated sources.

Figure 1 shows the 18 individual spectra. Silicate absorption can be found in most of the sources. In two cases (AMS 05: see the Appendix; AMS 17), the lack of this feature can be explained due to their high redshift, so the feature is expected to be centered

---

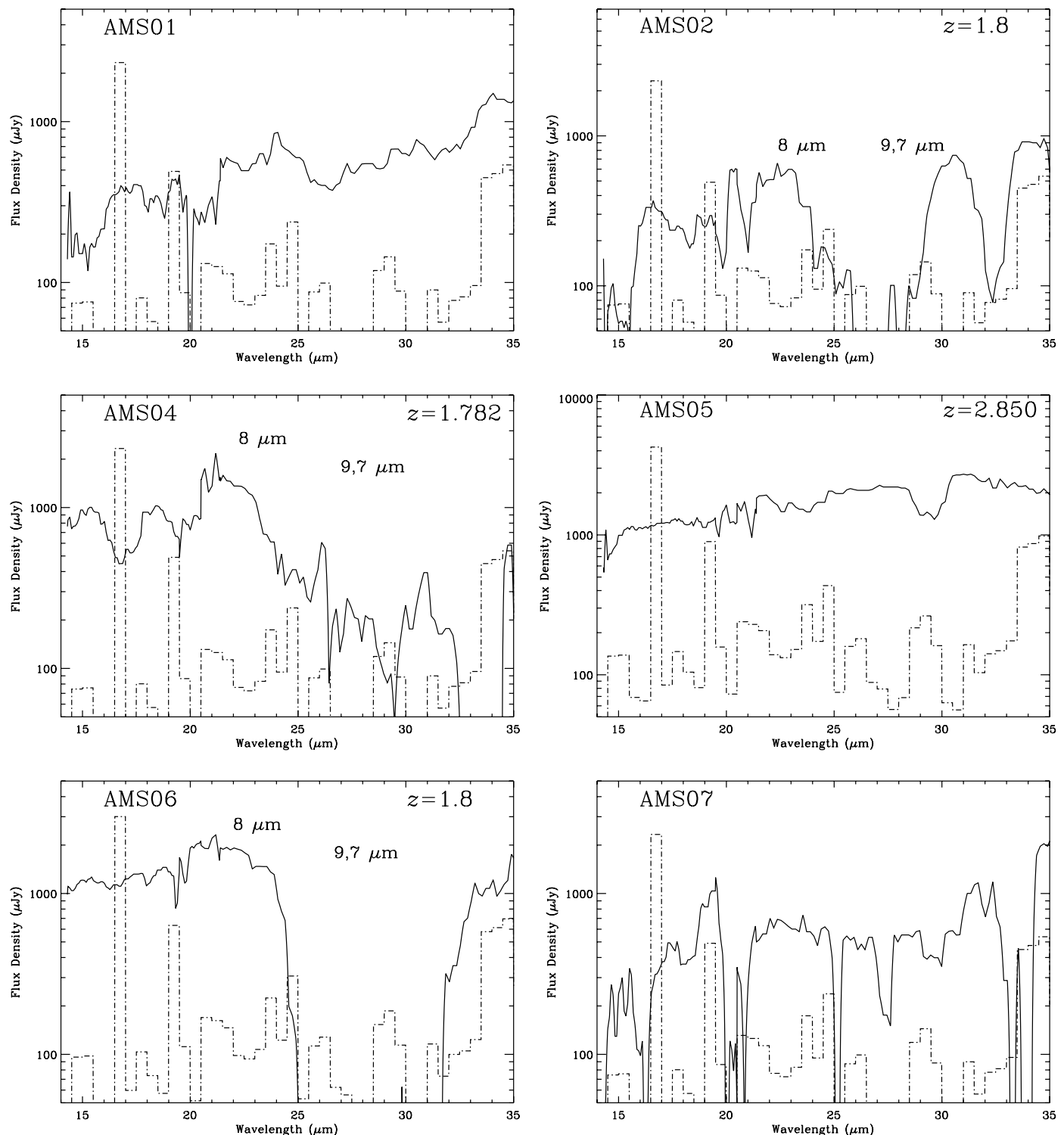[4] See http://ssc.spitzer.caltech.edu/postbcd/softwarehome.html.
[5] See footnote 4.

Fig. 1.—Individual mid-infrared spectra of all 18 sources observed. As a guide to the eye, the rms noise estimate is plotted as a dash-dotted histogram. It was obtained by extracting a spectrum from a blank region in a two-dimensional spectrum, and scaling it to the appropriate number of cycles. For sources with a spectroscopic redshift, this is quoted in the top right corner. The features used to derive a redshift are also indicated at the observed wavelength.

at an observed wavelength $\lambda_{\mathrm{obs}} \geq 37$ μm. In other sources the low S/N means it is difficult to see this feature clearly, although hints of it are seen in the two-dimensional and one-dimensional spectra. In addition, from Figure 1, it can be seen that AMS 01 could be at $z \sim 2.1$ and have a shallow silicate feature, but we do not consider this redshift secure, so we do not quote it in Table 1.

In total, 12/21 sources show no emission lines in the optical (rest-frame ultraviolet; see also the Appendix). The mid-infrared

spectra of these 12 sources are continuum dominated, and eight sources show the silicate absorption feature. These mid-infrared properties are characteristic of AGNs. In fact six sources showing no rest-frame ultraviolet lines are at redshifts where the Lyα falls in the optical range (that is, $z \geq 1.7$), and therefore have no Lyα detection down to $S_{\mathrm{Ly}\alpha} \lesssim 2 \times 10^{-20}$ W m^{-2}. We estimate the absorption to the broad-line region at 1216 Å to be $A_{\mathrm{Ly}\alpha} \sim$ 60–120 mag (see § 3.2). The extinction toward the narrow-line
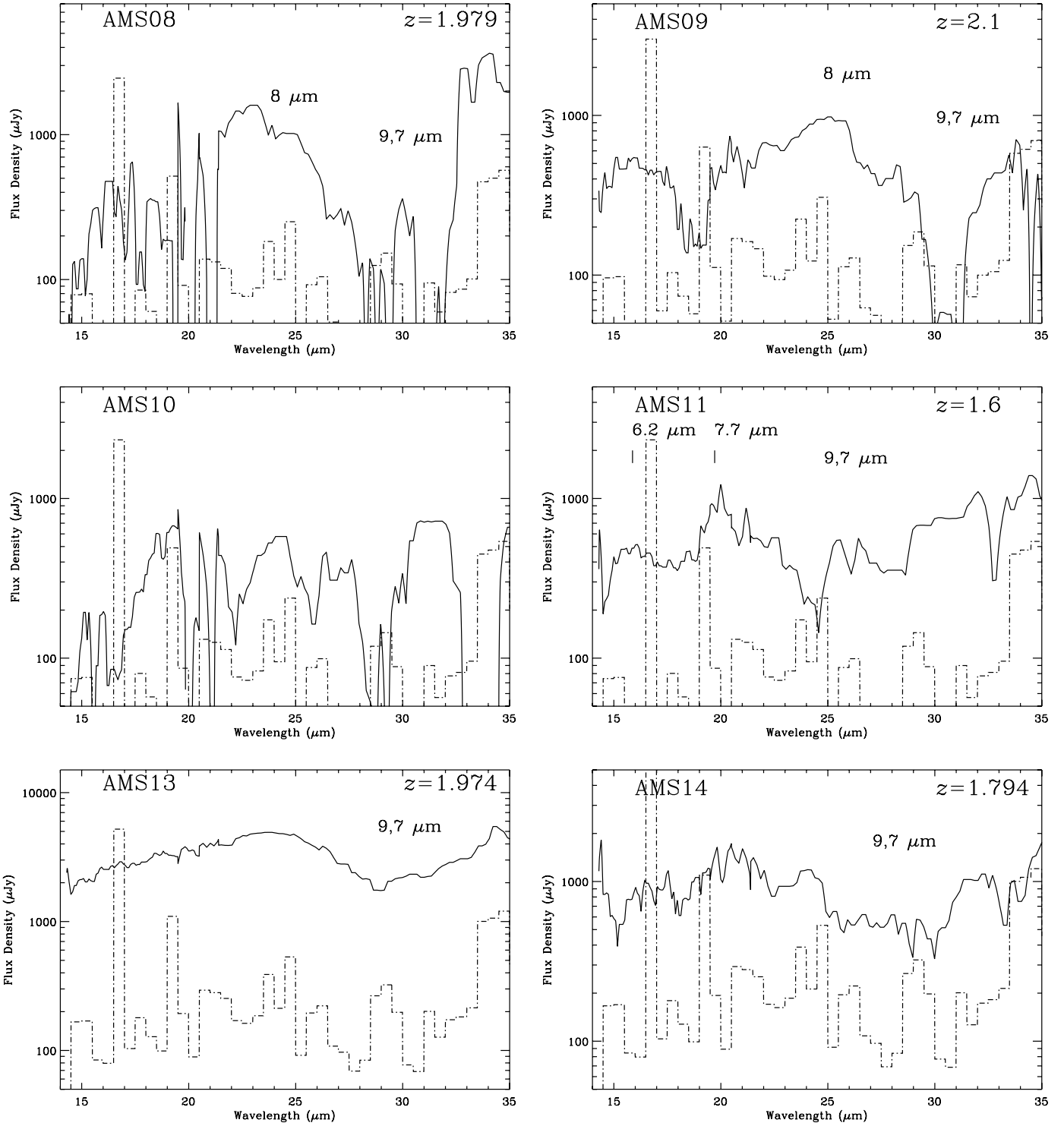
Fig. 1—*Continued*

region is expected to be significantly lower. However, the Lyα line suffers from resonant scattering, so modest amounts of dust mixed with the narrow-line region could still severely extinguish the line emission. Indeed, the Lyα profile of AMS 03 (Fig. 6 of Martínez-Sansigre et al. 2006b) is very similar to the simulated spectrum of a young dusty galaxy by Laursen & Sommer-Larsen (2007; their Fig. 2), which includes resonant scattering. AMS 03 is close to the limit of our sensitivity, so sources where the narrow-line region is dustier, or where the Lyα line is intrinsically less luminous than in AMS 03, will not show Lyα in our optical spectra.

We find 10 objects with an excess emission around rest frame 8 μm, which at first suggests the 7.7 μm PAH emission band. These objects are AMS 02, AMS 04, AMS 06, AMS 08, AMS 09, AMS 11, AMS 15, AMS 17, AMS 18, and AMS 21. Care must be taken, however, since for heavily absorbed sources, there is an apparent excess at 8 μm. This is due to the minimum in optical depth between the absorption features due to silicate, water ice (centered at 6.0 μm), and hydrogenated amorphous carbons (at 6.9 and 7.3 μm; for a detailed discussion, see Spoon et al. 2002). At first sight, this excess emission around 8 μm can
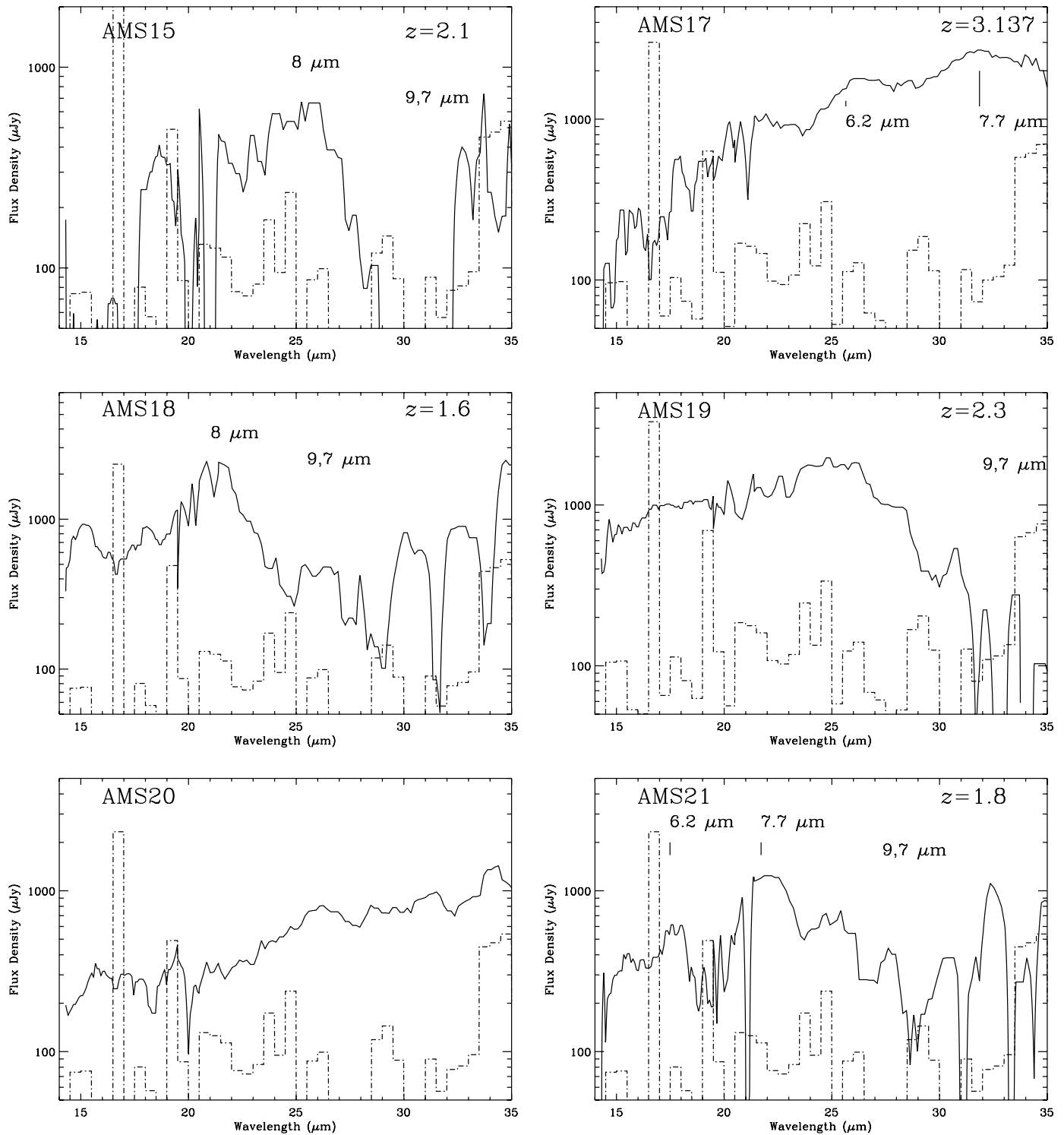
Fig. 1—*Continued*

mimic the 7.7 μm PAH, but it is wider than the 7.7 μm PAH, and it is not accompanied by the 6.2 μm PAH. In three sources (AMS 11, AMS 17, and AMS 21), there is a hint of another emission band corresponding to the 6.2 μm PAH. A mean spectrum of these three sources (hereafter subsample A) is shown in Figure 2*a*, where the 6.2 and 7.7 μm PAHs are detected. The mean spectrum of the remaining seven sources with a maximum around 8 μm, but no clear hint of the 6.2 μm PAH (subsample B), is shown in Figure 2*b*. Figure 2*c* shows the mean spectrum of subsample C, consisting of four sources (AMS 05, AMS 13,

AMS 14, and AMS 19) continuum dominated with clear silicate absorption, but no hint of excess emission around 7.7–8 μm. For reference, Figure 2 has the mid-infrared spectra of several low-redshift ultraluminous infrared galaxies (ULIRGs) overlaid (with $L_{IR} > 10^{12}~L_{\odot}$; from Armus et al. 2007; Spoon et al. 2007). These are: IRAS 12514+1027 (hereafter IRAS 12514), Mrk 231, Mrk 273, and Arp 220. The mid-infrared spectrum of IRAS 12514 represents a pure AGN, and Mrk 231 and Mrk 273 represent AGN-starburst composites, while in the mid-infrared, Arp 220 is starburst dominated.
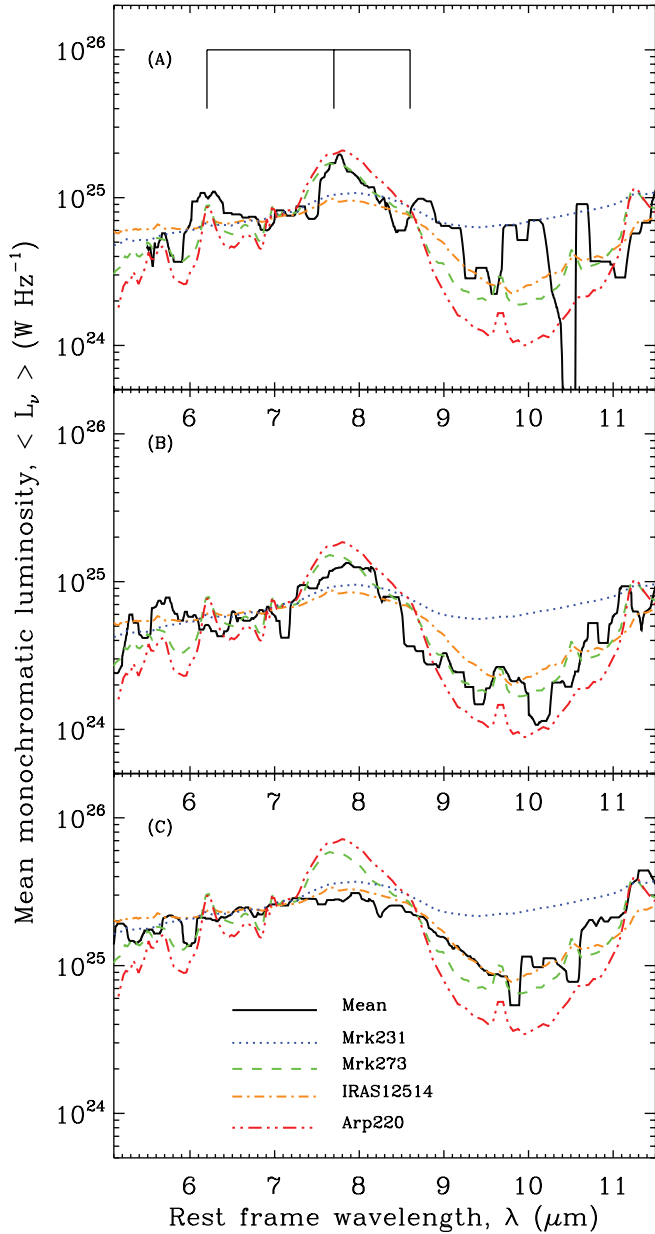
FIG. 2.— Mean mid-infrared spectra of the subsamples. Overlaid for reference are high-quality low-resolution mid-infrared spectra of four local ultraluminous infrared galaxies: Arp 220 (a starburst-dominated ULIRG), Mrk 273 and Mrk 231 (both AGN-starburst composites), and IRAS 12514+1027 (with an AGN-dominated spectrum). These are normalized to go through the data around 7 μm. Subsample A (*top*): Mean spectrum of three sources with both the 7.7 and 6.2 μm PAHs visible. The wavelength of these two PAHs, together with the 8.6 μm one, are marked with lines. Subsample B (*middle*): This includes seven objects with an excess around 8 μm; due to the lack of 6.2 μm PAH, these are not included in subsample A. The mean spectrum shows the excess emission to be very broad, and the 6.2 μm PAH is still not detected, suggesting this is due to the minimum in optical depth around 8 μm and not the 7.7 μm PAH. Subsample C (*bottom*): This consists of four sources with clear continuum, and no hint of an excess around 7 or 8 μm. The mean spectrum is well described by that of IRAS 12514.

For each subsample, the mid-infrared spectrum of IRAS 12514 was used as a continuum template. It was normalized using the mean luminosity density of the 6.5–7.5 μm region, and then subtracted. The residuals are plotted in Figure 3, with the spectrum of M82 (Sturm et al. 2000) overlaid as a reference for the location of the PAHs. Table 2 summarizes the mean PAH luminosities or limits for each subsample.
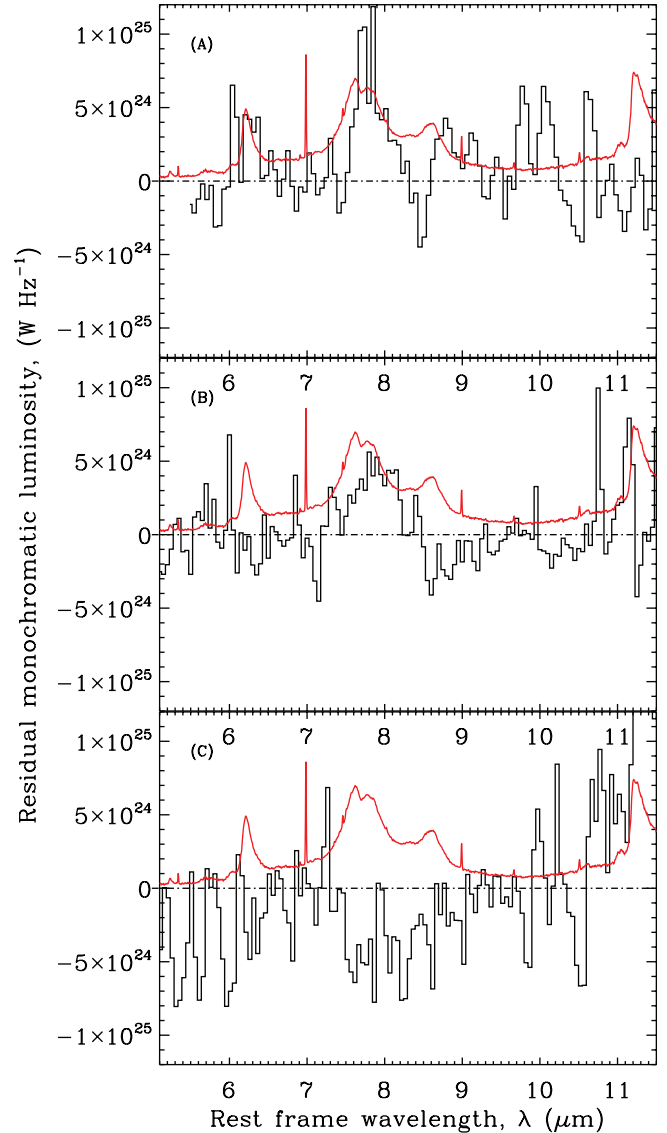

FIG. 3.— Residuals after subtracting the template of IRAS 12514 to the mean spectra of subsamples A (*top*), B (*middle*), and C (*bottom*). For reference, the mid-infrared spectrum of M82 is overlaid, which shows the expected positions of the 6.2, 7.7, and 8.6 μm PAHs. Subsample A has two regions of excess flux, compared to either template; these are at the exact wavelengths of the 6.2 and 7.7 μm PAHs, and have the correct width. Subsample B shows a broad excess centered at 8 μm, and no hint of the 6.2 μm PAH. Although the latter could be lost in the noise, the excess at 8 μm is probably best explained by continuum. Therefore, we do not consider subsample B to have a detection of the 7.7 μm PAH. Subsample C shows no residual, so the template provides a very good description. The region of 5.5–8.5 μm has lower noise than the region 8.5–11.5 μm, and of the two regions only the former is used to estimate the significance of the detections in Table 2.

In subsample A, there is a detection of the 6.2 μm PAH (3.4 σ; see Table 2) together with the 7.7 μm PAH (6.4 σ). The noise is calculated in the 5.0–8.5 μm region (note that this is lower than in the 8.5–11.5 μm region), and as is mentioned in Table 2, it is the noise in the 5.0–8.5 μm region that is used to estimate the significance of the detections. The uncertainty in the line flux additionally includes the uncertainty in the continuum subtraction. In subsample A the presence of PAHs is an indicator for ongoing star formation in the host galaxy.

Subsample B shows an excess around 8 μm but no hint of the 6.2 μm line. The shape of the excess, and the lack of the 6.2 μm

TABLE 2
ESTIMATED PAH STRENGTH AND SIGNIFICANCE

Subsample	$L_{bol}/10^{13}\ L_\odot$	$L_{6.2}/10^{10}\ L_\odot$[a]	Signif./σ[b]	$L_{7.7}/10^{10}\ L_\odot$[a]	Signif./σ[b]
A...........................	0.9	2.2 ± 1.8	3.4	4.6 ± 1.8	6.4
B...........................	0.8	≤5.4	≤3	≤5.4	≤3
C...........................	2.8	≤6.5	≤3	≤6.5	≤3

[a] The estimated uncertainties include both the uncertainty in removing the continuum and the noise of the residual.
[b] For detections we quote the significance of the lines above the noise of the residual; the uncertainty in removing the continuum is not included. For nondetections, we quote a 3 σ limit.

PAH, strongly suggest this excess at 8 μm is continuum and not the 7.7 μm PAH. Thus, in subsample B we conclude there is no evidence for PAHs, within our sensitivity, and that the maximum at 8 μm is probably continuum. Subsample C shows no hint of any PAH or any excess at 8 μm, and indeed the residuals in Figure 3c are consistent with noise. The mid-infrared spectrum of subsample C is, within our sensitivity, indistinguishable from that of IRAS 12514.

Wilman et al. (2003) obtained an X-ray detection of IRAS 12514, and estimated the total bolometric luminosity to be $L_{bol} \sim 1.6 \times 10^{13}\ L_\odot$, with a Compton-thick quasar and a powerful starburst contributing comparable fractions to L_{bol} (a source is Compton-thick if the absorbing column density, N_H, is $\geq 1/\sigma_T = 1.5 \times 10^{28}\ \text{m}^{-2}$, where σ_T is the Thomson electron scattering cross section). The mid-infrared spectrum of IRAS 12514, however, is AGN dominated, with a very low value of the 6.2 μm PAH equivalent width (see Fig. 1 of Spoon et al. 2007). Thus, although the mid-infrared spectra of samples B and C show no signs of starburst activity, vigorous ongoing star formation in the host galaxy cannot be ruled out.

3.2. Derived Extinctions

The spectra are noisy in the silicate region, and from Figure 3 it is clear that the derived depth of the absorption feature, $\tau_{9.7}$, will vary vastly depending on the exact wavelength at which it is measured and the choice of anchor for the continuum (see, e.g., Spoon et al. 2007). However, we can estimate $\tau_{9.7}$ by comparison with the local ULIRGs. Arp 220 has $\tau_{9.7} = 3.3$, Mrk 231 $\tau_{9.7} = 0.8$, and Mrk 273 $\tau_{9.7} = 1.8$ (all three from Armus et al. 2007), while IRAS 12514 has $\tau_{9.7} = 1.5$ (Spoon et al. 2007). For subsample A, in the silicate region, the spectra of Mrk 273 and Mrk 231 represent lower and upper envelopes, respectively, so $0.8 < \tau_{9.7} < 1.8$. For subsample B, IRAS 12514 provides an upper envelope, and Arp 220 provides a lower one (so $1.5 < \tau_{9.7} < 3.3$), while within the noise, the spectrum of Mrk 273 is a good fit, so $\tau_{9.7} \sim 1.8$. The spectrum of subsample C is very close to that of IRAS 12514, so $\tau_{9.7} \sim 1.5$.

We can see that $\tau_{9.7}$ is typically ~ 1–2. Assuming $A_V = 18.5\tau_{9.7}$ (Draine 2003), we therefore expect values of A_V in the range ~ 18.5–37. Using the Milky Way dust model of Pei (1992) one expects the extinction at 1216 Å to be $A_{Ly\alpha} \sim 60$–120 mag. This is an estimate of $A_{Ly\alpha}$ toward the central region (i.e., to the broad Lyα line).

Following Martínez-Sansigre et al. (2006b) we assume a gas-to-dust ratio of $N_H = 5 \times 10^{26}\ \text{m}^{-2}\ A_V$, which suggests column densities $\sim 9 \times 10^{27}$–$2 \times 10^{28}\ \text{m}^{-2}$. We compare this to the absorbing column densities of the AGNs in IRAS 12514, Mrk 231, and Mrk 273: Balestra et al. (2005) find $N_H = 7 \times 10^{27}\ \text{m}^{-2}$ in Mrk 273, while Wilman et al. (2003) find $N_H > 1.5 \times 10^{28}\ \text{m}^{-2}$ in IRAS 12514. For Mrk 231, Braito et al. (2004) estimate $N_H \sim 2 \times 10^{28}\ \text{m}^{-2}$. Thus, the low-redshift ULIRGs whose mid-

infrared spectra most resemble our sample are all AGNs heavily absorbed in X-rays, or even Compton-thick.

Indeed, the detection of PAHs in subsample A suggests the star-forming regions emitting the PAHs must be shielded from the X-rays, or else the PAHs would be destroyed (Voit 1992). The line of sight of the PAHs to the central source of X-rays is not necessarily the same as our line of sight, but there is a strong suggestion here that many of the sources in this sample will be Compton-thick, as was suggested also by Martínez-Sansigre et al. (2007).

The mid-infrared spectra can also be used to estimate the mean bolometric luminosity of each subsample. Assuming the 6.5–7.5 μm region is dominated by the AGN continuum, $L_{bol} \sim 10 \times \lambda L_\lambda \sim 10^{13}\ L_\odot$ (assuming and unobscured quasar spectral energy distribution [SED], following Elvis et al. [1994]). These sources are not, of course, unobscured quasars, but the effect of dust at 7 μm is small: we have estimated the range of A_V to be ~ 18.5–37. Using the Milky Way–type dust model of Pei (1992) the expected transmission at 7 μm is $\sim 60\%$–75% for this range of A_V, while it is $\sim 50\%$–55% for Small Magellanic Cloud–type dust. Hence, the bolometric luminosity is underestimated by at most 50%, which is smaller than or comparable to the intrinsic uncertainty in using the Elvis et al. (1994) conversion (which is a factor of ~ 2; see also Richards et al. 2006). Note that values of $L_{bol} \gtrsim 10^{13}\ L_\odot$ are also estimated for the sample of Martínez-Sansigre et al. (2007), which was selected using very similar criteria as well as broadband SED fitting.

3.3. Possible Selection Bias?

A source of concern is whether there is a selection effect in our sample: by being selected at 24 μm, it could be biased in favor of $z \sim 2$ sources with strong PAHs. To a certain extent this is inevitable, but we show in this section how the effect is minimal. In addition, a look at the spectra in Figure 1 shows such a selection effect has not heavily affected us.

At $z = 2$, the 7.7 μm PAH is almost perfectly centered on the MIPS 24 μm band. We estimate the mean contribution to the 24 μm flux density of a $L_{7.7} = 5 \times 10^{10}\ L_\odot$ PAH (from Table 2) at $z = 2$ to be $\sim 100\ \mu$Jy. This can clearly be important for a sample whose flux density limit is 300 μJy. Thus, at the lower flux density end, our sample could be biased in favor of sources with PAHs, yet we expect at most $\sim 30\%$ contribution of the PAH to the 24 μm flux density, and for sources with $S_{24} > 650\ \mu$Jy, the contribution of the PAH will be $\lesssim 15\%$, and therefore smaller than or comparable to the uncertainty in the flux density.

Among the faint sources, we do see cases in which the sources have been selected due to the maximum around 8 μm falling in the 24 μm band (e.g., AMS 02 and AMS 15; see Fig. 1). Yet, as we have discussed in § 3.1, without detection of the 6.2 μm line, we believe this 8 μm excess to be continuum and not the 7.7 μm PAH. We have only identified PAHs in AMS 11, AMS 17, and AMS 21.

In the case of AMS 11, the peak of the 7.7 μm PAH is at 20 μm, but the MIPS 24 μm band has a spectral response curve with a full width at half-maximum between 20.8 and 26.1 μm (Rieke et al. 2004). Hence, at most half of the 7.7 μm PAH flux falls in the band, so the PAH contribution is expected to be $\sim$50 μJy. AMS 11 has a 24 μm flux density, $S_{24} = 442$ μJy (24 μm flux densities from Martínez-Sansigre et al. 2005), so subtracting the PAH contribution one expects $S_{24} \sim 392$ μJy, enough to be inside our sample anyway. AMS 17 is at $z = 3.137$, so only the 6.2 μm PAH falls in the 24 μm band. It has $S_{24} = 1134$ μJy: clearly the PAHs have no effect in the inclusion of this source in our sample. AMS 21 is at $z = 1.8$, and the PAH falls entirely within the 24 μm band, but with $S_{24} = 720$ μJy the PAH-subtracted flux density is $S_{24} \sim 620$ μJy, enough to be included. A look at AMS 21 in Figure 1 suggests the continuum to be slightly lower than this estimate, around $S_{24} \sim 400$ μJy, but still bright enough to be included in the sample.

Overall, the spectra shown in Figures 1 and 2 show our sample is not contaminated by pure starbursts, and in any case the radio properties suggest all our sources contain AGNs: the sources have radio luminosities, $L_{1.4} \sim 10^{24}$ W Hz^{-1} sr^{-1}, several have flat- or gigahertz-peaked radio spectra (Martínez-Sansigre et al. 2006a), and many have radio cores detected (H.-R. Klöckner et al. 2008, in preparation).

4. THE QUASAR FRACTION REVISITED

We use our new mid-infrared spectra (and the new optical spectra in the Appendix) to revisit the quasar fraction at $z \sim 2$, following Martínez-Sansigre et al. (2005). Above $z = 1.7$, Lyα is potentially visible in optical spectroscopy, while in our mid-infrared spectra, the 9.7 μm silicate absorption feature is visible in the approximate range $1.4 \lesssim z \lesssim 2.6$. Thus, our spectroscopic completeness to both "host-obscured" and "torus-obscured" quasars should now be close to 100% in this range. Above $z \sim 2.6$ we are no longer complete to sources showing no emission lines in the optical spectra. Thus, we estimate the quasar fraction at $1.7 \leq z \leq 2.6$, where we expect to have close to 100% spectroscopic completeness. We note that objects with no narrow lines in the optical spectrum and with shallow silicate absorption features could still be missing from our census (e.g., AMS 01 might be at $z \sim 2.1$, as discussed in § 3.1).

We begin by estimating the number of type 1 quasars following our 24 μm and radio criteria. This is estimated by using the Wolf et al. (2003) luminosity function (LF; assuming pure luminosity evolution [PLE]), together with a typical type 1 SED (essentially flat in νL_ν in the infrared; from Rowan-Robinson 1995), to estimate the number of $1.7 \leq z \leq 2.6$ type 1 quasars meeting our 24 μm cut. The optical-to-radio correlation of Cirasuolo et al. (2003) is then used to see what fraction of these type 1s would also meet the radio cuts. We estimate the errors by changing from PLE, to pure density evolution (PDE). We also vary the mid-infrared spectral index (where $L_\nu \propto \nu^{-\alpha_{MIR}}$) of the typical type 1 SED, assumed to be $\alpha_{MIR} = 1$, in the range $0.87 \leq \alpha_{MIR} \leq 1.13$, and the radio spectral index, assumed to be $\alpha_{rad} = 0.8$, in the range $0.5 \leq \alpha_{rad} \leq 1$. The errors are then added in quadrature, with the difference between PDE and PLE considered as a ± 1 σ error, while the range spanned by the spectral indices is considered to be ± 2 σ. In an area of 3.8 deg^2, we predict $6.0^{+2.3}_{-1.4}$ such type 1 quasars.

Our sample includes four objects with spectroscopic redshifts $1.7 \leq z \leq 2.6$ from rest-frame ultraviolet lines in the optical spectra. A further six objects have $1.7 \leq z \leq 2.6$ from the mid-infrared spectra (see Table 1). Figure 4 shows the normalized
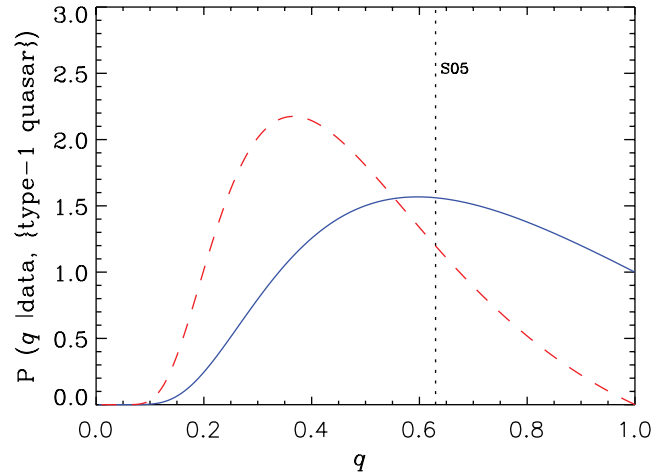

FIG. 4.—Posterior probability distribution function of the quasar fraction, q, in the redshift range $1.7 \leq z \leq 2.6$, given our data and given our modeled number of type 1 quasars. The solid blue line shows the distribution if we only use type 2 quasars showing lines in the optical spectra (corresponding to rest-frame ultra-violet), while the dashed red line shows the case in which spectroscopic redshifts from *Spitzer* IRS have been used to complement the optical redshifts. Note that only spectroscopically confirmed type 2 quasars are used. The small number of sources used to derive the solid blue curve leads to a large error, so that the probability of $q \geq 1$ is not zero. For the dashed red line, the number of sources used is large enough to avoid this problem. The vertical line labeled S05 marks the prediction of the Simpson (2005) receding torus model, which should only be compared to the solid blue line.

posterior probability distribution of the quasar fraction, q, given our data, given the modeled number of type 1 quasars, and assuming a prior probability distribution for the quasar fraction flat in the entire possible parameter range of $0 \leq q \leq 1$ (again, following Martínez-Sansigre et al. 2005). The solid blue line shows the quasar fraction when only the type 2 quasars with optical redshifts are used (four type 2s for a predicted 6.0 type 1s): it has a modal value of 0.60, and 68% of the area lies in the region with $q \geq 0.51$ (note that, for this curve, the errors are so large that the probability of $q > 1.0$ is greater than zero). The dashed red line shows the posterior distribution for q when all 10 type 2 quasars are considered: it has a modal value of 0.37, and the region $0.23 \leq q \leq 0.59$ encompasses 68% of the area.

We summarize the derived quasar fraction as $q = 0.60^{+0.40}_{-0.09}$ for type 2 quasars showing narrow lines only, and $q = 0.37^{+0.22}_{-0.14}$ for all type 2 quasars with spectroscopic redshifts. The "receding-torus" model of Simpson (2005) marked "S05," was derived from type 1 and type 2 AGNs showing emission lines, and should only be compared to the solid blue line of Figure 4. His model predicts a value of $q = 0.63$ at high AGN luminosities, in good agreement with our results.

We stress that the uncertainties are still large. For example, if instead we derive the quasar fraction at all $z \geq 1.7$, we estimate $6.7^{+3.0}_{-2.2}$ type 1 quasars, and the two quasar fractions as $q = 0.45^{+0.24}_{-0.16}$ (using only type 2 quasars with narrow lines and $z_{spec} \geq 1.7$) and $q = 0.32^{+0.19}_{-0.12}$ (using all type 2 quasars with $z_{spec} \geq 1.7$). However, for the range $1.7 \leq z \leq 2.6$, where our spectroscopic completeness is highest, our best estimate of the radio-intermediate quasar fraction is $q = 0.37^{+0.22}_{-0.14}$, or, equivalently, 63^{+14}_{-22}% of radio-intermediate quasars are obscured.

5. COMPARISON WITH OTHER HIGH-REDSHIFT SAMPLES

Searches for PAHs in high-redshift (unobscured) quasars have proven difficult: Maiolino et al. (2007) observe a sample of 25
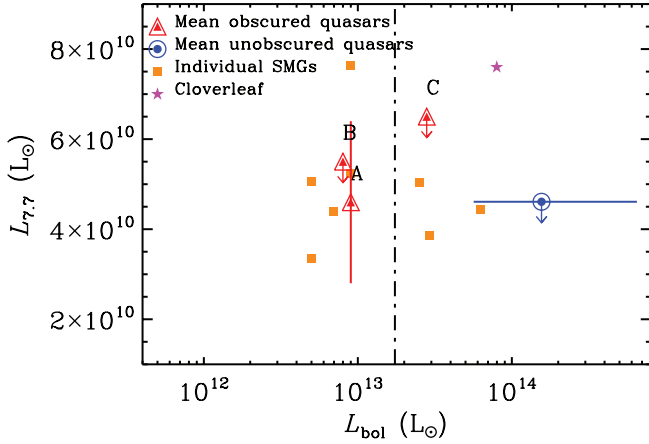
FIG. 5.—Luminosity of the 7.7 μm PAH line $L_{7.7}$ vs. bolometric luminosity L_{bol} (both in solar luminosities) for samples of $z \sim 2$ quasars and SMGs with comparable mid-infrared spectroscopy. Upper limits are 3 σ. Our sample of $z \sim 2$ obscured quasars is represented by two points: the mean value for detections (Fig. 2a) and the upper limit from the nondetections (Figs. 2b–2c). The unobscured quasars are from the sample of Maiolino et al. (2007), the "Cloverleaf" quasar is from Lutz et al. (2007), and the SMGs are from Valiante et al. (2007). The vertical dashed line represents the break of the unobscured quasar LF (Croom et al. 2004), converted to L_{bol} using the SED of Elvis et al. (1994). This should only be compared to quasars (both obscured and unobscured), but not to SMGs.

optically bright $z \sim 2$–3 quasars, find no detection even in their stacked spectrum, and derive an upper limit on the luminosity of the 7.7 μm PAH, $L_{7.7} \leq 4.6 \times 10^{10}$ $L_{\odot}$. The sources comprising the sample of Maiolino et al. (2007) have bolometric luminosities significantly larger than those of our own sample, making the PAHs difficult to see over the strong continuum. However, this is a good comparison sample, as it is unbiased in terms of the star formation rates (SFRs) in the host galaxies.

Lutz et al. (2007) do find a detection in the "Cloverleaf" quasar, with $L_{7.7} = 7.6 \times 10^{10}$ $L_{\odot}$, although this is a biased case, since it was observed because of its being hyperluminous in the far-infrared (even after correction for gravitational magnification).

In Figure 5 the PAH strengths and estimated bolometric luminosities of subsamples A, B, and C are compared to those of the unobscured quasars mentioned above and the sample of submillimeter-selected galaxies (SMGs) of Valiante et al. (2007). The SMGs represent the most powerful starbursts known, and have their bolometric luminosities approximated to their total infrared luminosities (from Valiante et al. 2007). Detection of the PAH is not an artifact of any selection criteria other than SMGs being galaxies with vigorous star formation.

Our sample of obscured quasars is around the break in the LF (Croom et al. 2004), so these sources represent the bulk of the energy density (or accreted mass density) of SMBHs. However, they are radio-intermediate (with $L_{1.4GHz} \sim 10^{24}$ W Hz^{-1} sr^{-1}), and therefore are more rare in space density than genuinely radio-quiet obscured quasars. In addition, this radio selection could possibly affect the observed properties, something that must be kept in mind. If the quasars were obscured solely by the torus of the unified schemes, the luminosity of the PAHs from star formation in the quasar host galaxies should be similar for unobscured and obscured quasars.

In our sample, emission from PAHs is detected in 3 out of 18 objects observed (subsample A). For this subsample, the inferred values of $L_{7.7}$ are similar to those of the SMGs, and only slightly lower than the value of the Cloverleaf. The limits inferred for nondetections (both for subsamples B and C and the unobscured quasars of Maiolino et al. [2007]) are similar to the values of the

detections, so little can be said about any differences in PAH properties between samples.

The obscured quasars with detections of PAHs have similar values of $L_{7.7}$ to the SMGs, which are powerful starbursts. The actual conversion from $L_{7.7}$ to a SFR is more uncertain, since for higher luminosity starbursts $L_{7.7}$ does not increase linearly with the far-infrared luminosity (Haas et al. 2001; Klaas et al. 2001; Dale & Helou 2002). Although it is difficult to estimate the SFRs from $L_{7.7}$, the values of $L_{7.7}$ estimated for obscured quasars are similar to those of SMGs (see Fig. 5), which have typical SFRs $\gtrsim 1000$ $M_{\odot}$ yr^{-1} (of all stars, integrated over a Salpeter initial mass function) estimated from their rest-frame far-infrared luminosities. These values of $L_{7.7}$ are, in addition, larger than the limits inferred for lower redshift X-ray-absorbed quasars (Sturm et al. 2006), or the values of $L_{7.7}$ found in nearby "PG" quasars (Schweitzer et al. 2006), which have lower far-infrared luminosities and thus inferred SFRs ($\lesssim 100$ $M_{\odot}$ yr^{-1}) than the SMGs.

6. CONCLUSIONS

Two main conclusions can be extracted from this work. First, we have found that the mid-infrared spectra are continuum dominated, and 12 out of 18 spectra show a deep silicate absorption feature (with $\tau_{9.7} \sim 1$–2). We have confirmed spectroscopically the existence of sources with mid-infrared spectra characteristic of heavily obscured quasars, but that do not show rest-frame ultraviolet emission lines (observed in the optical). The number of these sources is similar to the number of obscured quasars that do show ultraviolet narrow emission lines. Using the new mid-infrared redshifts, we confirm that the population of radio-intermediate obscured (type 2) quasars outnumbers the unobscured population (type 1), and that 63^{+14}_{-22}% of $z \sim 2$ radio-intermediate quasars are obscured. This had already been suggested in Martínez-Sansigre et al. (2005), and in this paper we confirm the result spectroscopically: among radio-intermediate sources, the population of obscured quasars is responsible for the bulk of the accretion onto supermassive black holes.

Second, we have found that obscured quasars are sometimes hosted by galaxies undergoing vigorous star formation, with detectable PAHs comparable in strength to those found in SMGs. The accompanying SFR is expected to be very large ($\gtrsim 100$ $M_{\odot}$ yr^{-1}), so that it can form a significant fraction of an L_K^* galaxy in $\sim 10^7$–10^8 yr. The dust and gas fueling this star formation are likely to be responsible for at least part of the obscuration in some of the sources, with the accreting black hole deeply embedded. These properties are those expected from an obscured phase of black hole growth (Fabian 1999), and could explain why in some obscured quasars the rest-frame ultraviolet lines are not detectable.

APPENDIX

NEW OPTICAL SPECTRA

For AMS 18, the redshifts derived from optical and mid-infrared spectroscopy disagree completely (compare our Table 1 to Table 1 of Martínez-Sansigre et al. [2006b]), and AMS 15 had not been observed in optical spectroscopy. AMS 03 was found to have an interesting source nearby: in imaging data, the source was pointlike in K, but galaxy-like in R, suggesting a reddened quasar. For these reasons the three objects were observed using the ISIS spectrograph at the William Herschel Telescope in 2007 July.

In the spectrum of AMS 18 reported in Martínez-Sansigre et al. (2006b) three very weak lines were visible, at 4680, 5652, and 7527 Å, yet our new spectrum shows no hint of these three lines. Thus, it is most likely that they were not real and the redshift reported in Martínez-Sansigre et al. (2006b) is incorrect. Thus, we favor the redshift of $z = 1.6$ from mid-infrared spectroscopy, and this value is quoted in Table 1.

In AMS 15 we find no evidence for any optical lines, in either the blue or red spectra. For AMS 03, the slit was placed at a different position angle ($31°$) to go through the reddened quasar. In the one-dimensional spectrum of AMS 03, we see the same double-peaked emission as reported in Martínez-Sansigre et al. (2006b; their Fig. 6). The optical spectrum of the candidate reddened quasar looks like that of an elliptical galaxy at $z = 0.7$, and no obvious emission lines are visible.

In addition, for AMS 05, a new optical spectrum and imaging (using both narrow and broad bands) suggest the Lyα line had been misidentified as C IV, and the object is actually at $z = 2.850$ rather than at $z = 2.017$ (D. Smith 2007, private communication).

Comparing optical and mid-infrared spectral properties, and radio properties, we see that none of the sources with flat radio spectra show narrow lines in their optical spectra (AMS 07, AMS 15, AMS 18, and AMS 19; see Table 1). This is important, as from unified schemes, one expects flat-spectrum radio sources to have broad lines (except in the case of blazars, where the beamed continuum can outshine the broad-line region). Thus, if these sources are obscured, the obscuration must occur due to dust on a larger scale (not due to the torus), and so the narrow lines, as well as the broad lines, are expected to be obscured. Alternatively, the dust might be on a small scale similar to that of the torus, but with a covering fraction ~ 1, so that the narrow-line region cannot be excited by photons from the central engine.

REFERENCES

Aitken, D. K., & Roche, P. F. 1985, MNRAS, 213, 777
Alonso-Herrero, A., et al. 2006, ApJ, 640, 167
Antonucci, R. 1993, ARA&A, 31, 473
Armus, L., et al. 2007, ApJ, 656, 148
Balestra, I., Boller, T., Gallo, L., Lutz, D., & Hess, S. 2005, A&A, 442, 469
Benson, A. J., Bower, R. G., Frenk, C. S., Lacey, C. G., Baugh, C. M., & Cole, S. 2003, ApJ, 599, 38
Braito, V., et al. 2004, A&A, 420, 79
Brand, K., et al. 2007, ApJ, 663, 204
Cirasuolo, M., Celotti, A., Magliocchetti, M., & Danese, L. 2003, MNRAS, 346, 447
Clavel, J., et al. 2000, A&A, 357, 839
Croom, S. M., Smith, R. J., Boyle, B. J., Shanks, T., Miller, L., Outram, P. J., & Loaring, N. S. 2004, MNRAS, 349, 1397
Dale, D. A., & Helou, G. 2002, ApJ, 576, 159
Donley, J. L., Rieke, G. H., Rigby, J. R., & Pérez-González, P. G. 2005, ApJ, 634, 169
Draine, B. T. 2003, ARA&A, 41, 241
Elvis, M., et al. 1994, ApJS, 95, 1
Fabian, A. C. 1999, MNRAS, 308, L39
Ferrarese, L., & Merritt, D. 2000, ApJ, 539, L9
Haas, M., Klaas, U., Müller, S. A. H., Chini, R., & Coulson, I. 2001, A&A, 367, L9
Houck, J. R., et al. 2004, ApJS, 154, 18
Klaas, U., et al. 2001, A&A, 379, 823
Lacy, M., Petric, A. O., Sajina, A., Canalizo, G., Storrie-Lombardi, L. J., Armus, L., Fadda, D., & Marleau, F. R. 2007, AJ, 133, 186
Lacy, M., et al. 2004, ApJS, 154, 166
Laursen, L., & Sommer-Larsen, J. 2007, ApJ, 657, L69
Lutz, D., et al. 2007, ApJ, 661, L25
Magorrian, J., et al. 1998, AJ, 115, 2285
Maiolino, R., Shemmer, O., Imanishi, M., Netzer, H., Oliva, E., Lutz, D., & Sturm, E. 2007, A&A, 468, 979
Martínez-Sansigre, A., Rawlings, S., Garn, T., Green, D. A., Alexander, P., Klöckner, H.-R., & Riley, J. M. 2006a, MNRAS, 373, L80

Martínez-Sansigre, A., Rawlings, S., Lacy, M., Fadda, D., Jarvis, M. J., Marleau, F. R., Simpson, C., & Willott, C. J. 2006b, MNRAS, 370, 1479
Martínez-Sansigre, A., Rawlings, S., Lacy, M., Fadda, D., Marleau, F. R., Simpson, C., Willott, C. J., & Jarvis, M. J. 2005, Nature, 436, 666
Martínez-Sansigre, A., et al. 2007, MNRAS, 379, L6
Pei, Y. C. 1992, ApJ, 395, 130
Richards, G. T., et al. 2006, ApJS, 166, 470
Rieke, G. H., et al. 2004, ApJS, 154, 25
Roche, P. F., Aitken, D. K., Smith, C. H., & Ward, M. J. 1991, MNRAS, 248, 606
Rowan-Robinson, M. 1995, MNRAS, 272, 737
Sajina, A., Yan, L., Lacy, M., & Huynh, M. 2007, ApJ, 667, L17
Schweitzer, M., et al. 2006, ApJ, 649, 79
Siebenmorgen, R., Krügel, E., & Spoon, H. W. W. 2004, A&A, 414, 123
Silk, J., & Rees, M. J. 1998, A&A, 331, L1
Simpson, C. 2005, MNRAS, 360, 565
Spoon, H. W. W., Keane, J. V., Tielens, A. G. G. M., Lutz, D., Moorwood, A. F. M., & Laurent, O. 2002, A&A, 385, 1022
Spoon, H. W. W., Marshall, J. A., Houck, J. R., Elitzur, M., Hao, L., Armus, L., Brandl, B. R., & Charmandaris, V. 2007, ApJ, 654, L49
Sturm, E., Hasinger, G., Lehmann, I., Mainieri, V., Genzel, R., Lehnert, M. D., Lutz, D., & Tacconi, L. J. 2006, ApJ, 642, 81
Sturm, E., Lutz, D., Tran, D., Feuchtgruber, H., Genzel, R., Kunze, D., Moorwood, A. F. M., & Thornley, M. D. 2000, A&A, 358, 481
Valiante, E., Lutz, D., Sturm, E., Genzel, R., Tacconi, L. J., Lehnert, M. D., & Baker, A. J. 2007, ApJ, 660, 1060
Voit, G. M. 1991, ApJ, 379, 122
———. 1992, MNRAS, 258, 841
Werner, M. W., et al. 2004, ApJS, 154, 1
Wilman, R. J., Fabian, A. C., Crawford, C. S., & Cutri, R. M. 2003, MNRAS, 338, L19
Wolf, C., Wisotzki, L., Borch, A., Dye, S., Kleinheinrich, M., & Meisenheimer, K. 2003, A&A, 408, 499